Multi-physics design optimization of a GaN based integrated modular motor drive system

M Uğur, O Keysan

Department of Electrical and Electronics Engineering, Middle East Technical University, Ankara, Turkey
ugurm@metu.edu.tr keysan@metu.edu.tr

Keywords: integrated motor drive, modular motor, permanent magnet synchronous machine, Gallium Nitride, interleaving

Abstract

In this paper, a multi-physics approach is presented for the design optimization of an integrated modular motor drive (IMMD). The system is composed of a modular permanent magnet synchronous motor and a GaN based modular motor drive power stage. The multi-physics model includes motor drive inverters and DC link capacitor bank (electrical model), stator windings and rotor magnets (electromagnetic model), heat sink (thermal model) and a geometrical model. The main purpose of the design optimization is to obtain the highest power density possible, which is quite critical in integrated drives. Due to the integrated structure, the system has several interdependencies and parameters are selected based on those relationships. An 8 kW IMMD system design is proposed and the resultant system design is verified using various simulation platforms.

1 Introduction

Conventional variable frequency motor drives are composed of two distinct parts: drive and motor, where the drive unit(s) are placed in separate cabinets and connected to the corresponding motors with long cables. This reduces the power density, increases cost and causes electromagnetic interference (EMI) problems [1]. In integrated modular motor drive (IMMD) systems, the drive is integrated onto the motor back iron forming a single package such that the power density of the overall system is increased and the connection cables are eliminated [1]. Furthermore, each pole of the motor is driven by its own drive module which are then interconnected via a common DC link. By doing so, the fault tolerance of the system is increased, heat dissipation is spread on a wider surface area and voltage stress on windings and power semiconductor devices are reduced [2].

In IMMDs, the space available for the drive system components is drastically reduced due to integration. Therefore, fitting all the components requires design optimization with integrated model approach and careful spatial and layout design. Moreover, the interdependencies between the main system components yields a multi-physics approach where the design of motor, drive power electronics and thermal management system should be considered all together. Therefore, it is highly difficult to propose a decoupled design approach in integrated drives as one parameter may affect the other significantly.

The current IMMD prototypes proposed in the literature are usually based on the new generation wide band-gap power semiconductor devices, such as Gallium Nitride (GaN) power FETs [3]. These devices are capable of switching at much higher switching frequencies compared to their silicon counterparts thanks to their low switching losses [3]. It is possible to reduce the size of passive components with high switching frequencies as well as reduce the size of heat sink with superior efficiency values with the utilization of enhancement mode (e-mode) GaNs. Considering that the largest components on an average power converter system are passive components and the heat sink [1], utilization of these devices is critical for IMMD designs. Moreover, thanks to the modularity of the system, interleaving technique can be used to further reduce the size of DC link capacitor bank [4]. Although several studies have been published regarding power electronics design, modular inverter topologies, DC link capacitor selection etc. for IMMDs [1,3,5], most of these prototypes lack a unified design procedure. One example for such a dependency is that, the cross-sectional area available for the motor drive printed circuit board (PCB) and heat sink is determined by the diameter of the motor.

In this paper, the optimum design of an 8kW IMMD system is presented considering both the motor and drive parameters to obtain the highest power density. It is also aimed to maximize the overall system efficiency while keeping the active material costs in acceptable limits. A permanent magnet synchronous motor (PMSM) having fractional slot concentrated winding (FSCW) stator is utilized for its superior torque density and fault tolerance capability which makes it suitable for IMMD applications [6]. The content of the multi-physics design optimization approach includes electrical, electromagnetic, thermal and geometrical models. First, the multi-physics model is presented in Section 2. In section 3, the basic relations between the system parameters and the cost and constraint functions are obtained and the inter-dependencies are discussed. Using the results of Section 3, an optimum system design is proposed in Section 3. In Section 4, the presented models are verified and the proposed system design is evaluated using simulation results. The paper is concluded in Section 5.

2 System modelling

Motor drive integration onto the modular stator back iron is considered in this paper, an example of which is shown in Fig. 1 [5]. The structural configuration of the proposed system is also shown in Fig. 2.

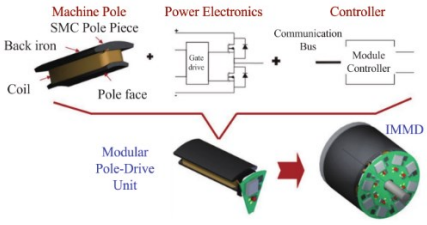

Figure 1. An example of the IMMD structure [5]

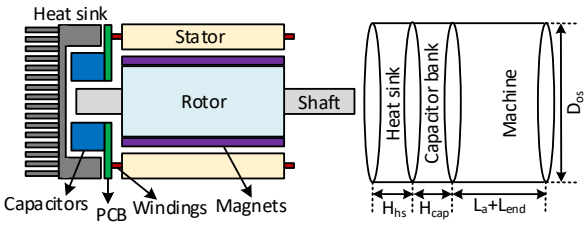

Figure 2. Structural configuration of the proposed IMMD

The main blocks of the system model and the relations between different aspects used in the integrated design are shown in Fig. 3. Basically, the system is composed of the electrical model, electromagnetic model, thermal model and geometrical (spatial) model. The system specifications and constraints are listed in Table 1. Moreover, the independent variables and their corresponding sub-models are also shown in Table 2. The IMMD system has a modular structure where each three-phase inverter module drives its own part of the stator pole. The modules can be connected in series and/or parallel configuration via a common DC link. A block diagram of the system is shown in Fig. 3 with 2-series and 2-parallel connected modules.

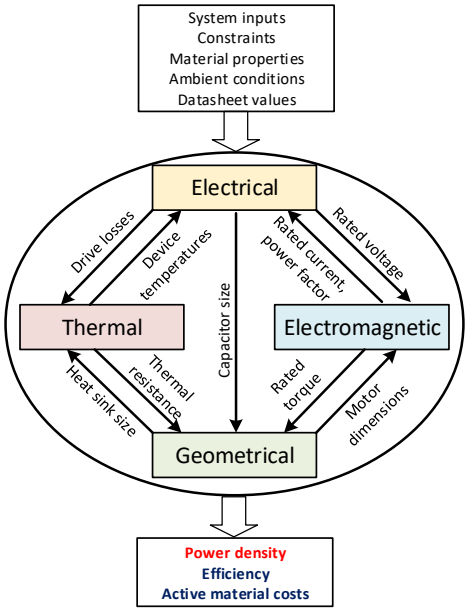

Figure 3. Main blocks of the system model

Parameter	Value
DC link voltage, V_{dc}	540 V
Number of phases in each module, m	3
Motor total output power, P_{out}	8 kW
Motor rated speed, N_r	600 rpm
Machine electric loading, A_{rms}	35 kA/m
Machine magnetic loading, B_{avg}	0.6 T
Maximum winding current density, J_{rms}	4 A/mm^2
Maximum stator teeth flux density, B_{ts}	1.8 T
Maximum stator yoke flux density, B_{ys}	1.4 T
Maximum fill factor, k_{cu}	0.6
Maximum device junction temperature, $T_{j\text{-}max}$	150 ^{0}C
Maximum capacitor temperature, $T_{cap\text{-}max}$	70 ^{0}C
Maximum DC link voltage ripple, $V_{dc\text{-}r}$	1 %
Minimum motor efficiency, $\eta_{m\text{-}min}$	94 %
Minimum drive efficiency, $\eta_{d\text{-}min}$	98 %
Minimum power factor, $cos(\varphi)_{min}$	0.9
Ambient temperature, T_{amb}	50 ^{0}C

Table 1. System specifications and constraints

Optimization parameters	Sub-model
Number of modules, n	*Electrical*
Number of series modules, n_s	*Electrical*
Switching frequency, f_{sw}	*Electrical*
Modulation index, m_a	*Electrical*
Aspect ratio of the motor, α	*Geometrical*
Slot/module/phase, w_s	*Electromagnetic*

Table 2. Optimization parameters (independent variables)

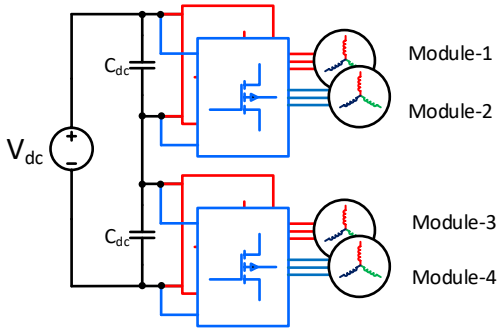

Figure 3. A general block diagram of the IMMD

2.1 Electrical sub-model

The electrical model selects rated parameters of the motor drive inverter, power semiconductor devices, calculates motor drive losses and required DC link capacitor parameters. A set of 650V e-mode GaN FETs suitable for high voltage applications having different current ratings from GaN Systems are used for the design [7]. The devices are selected from these commercial products based on the number of series and parallel modules (n_s, n_p), modulation index (m_a), power factor ($cos(\varphi)_{min}$) and motor efficiency ($\eta_{m\text{-}min}$) limitations. By using the selected device parameters, the motor drive losses are determined as shown in (1) for forward conduction loss, (2) for reverse conduction loss, (3) for switching loss, where E_{on}, E_{off}

and E_{oss} are the on state, off state and output capacitance switching energies, respectively, $R_{ds\text{-}on}$ is the on state resistance, I_p is the peak line current.

$$P_{cf} = {I_p}^2 R_{ds-on} [1/8 + m_a \cos(\varphi)_{min}/(3\pi)] \quad (1)$$

$$P_{cr} = {I_p}^2 R_{ds-on} [1/8 - m_a \cos(\varphi)_{min}/(3\pi)] \quad (2)$$

$$P_{sw} = [E_{on} + E_{off} + E_{oss}] \, f_{sw}/\pi \quad (3)$$

The analytical models for the determination of required capacitance (C_{dc}) and RMS current rating ($I_{c\text{-}rms}$) for a typical inverter are given in (4) and (5), where I_{rms} is the rms line current [4]. For a modular motor drive, it is possible to use interleaving technique to reduce these requirements. The effect of interleaving is determined by proper phase shifting angle for each possible case and added to the capacitance and ripple current requirements. It has been shown that series connection has no effect on the ripple current and ripple voltage for any phase shifting angle. The normalized effect of interleaving on these parameters is shown in Fig. 5.

$$C_{dc} = \frac{I_{rms} m_a}{16 f_{sw} V_{dc-r}} \sqrt{(6 - 96\sqrt{3}/5\pi + 9{m_a}^2/2)\cos(\varphi)^2 + 8 m_a \sqrt{3}/5\pi} \quad (4)$$

$$I_{c,rms} = I_{rms} \sqrt{\left[2m_a \left(\sqrt{3}/4\pi + \cos(\varphi)^2 (\sqrt{3}/\pi - 9m_a/16)\right)\right]} \quad (5)$$

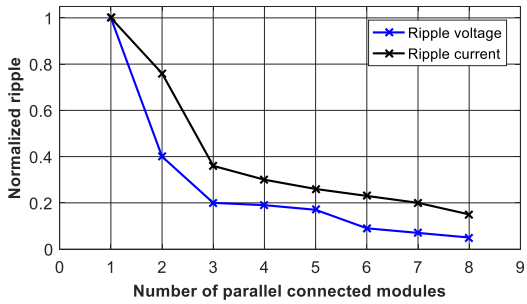

Figure 5. The effect of interleaving for parallel connected modules

A database of film capacitors are used from commercial products [8] for capacitor selection model which is based on the capacitance, ripple current and DC voltage requirements. The selected capacitor is checked whether its core temperature exceeds the specified limit or not, by using the implicit thermal model expressed in [8] and capacitor datasheet values such as ESR, thermal conductance etc. Temperature dependency is especially critical since it affects the lifetime of the capacitors significantly. The required phase induced voltage per module (E_{phm}), which is the link between the electrical and electromagnetic models is determined using the inverter model as in (6).

$$E_{phm} \approx 0.612 \, m_a \, V_{dc} \cos(\varphi)_{min}/(\sqrt{3} n_s) \quad (6)$$

2.2 Electromagnetic sub-model

This section summarized the electromagnetic design of a PMSM for the IMMD application. The number of stator slots (Q_s) is determined by using w_s, m and n. The machine stator structure is FSCW as it is more suitable for high torque modular motor applications thanks to its high power density and torque density, low cogging torque, low manufacturing cost and fault tolerance capability. The number of poles (p) is determined for each possible Qs to get low cogging torque while keeping the winding factor high enough and harmonic content at minimum. Tables with pre-determined winding factor values (k_w) for different Qs/p combinations are used for winding factor [6].

The air gap distance (l_g) is found using the target peak air gap flux density (B_{gp}) and the properties of the selected magnet ($NeFeB$) as in (7), using the lumped parameter magnetic circuit model shown in Fig. 6, where l_m is the magnet length. The same methodology is used for the determination of tooth width (b_t) and back core height (h_{bc}) using the maximum allowable flux density ($B_{ts\text{-}max}$ and $B_{ys\text{-}max}$), as in (8) and (9), where e_m is the magnet embrace and D_{is} is the bore diameter.

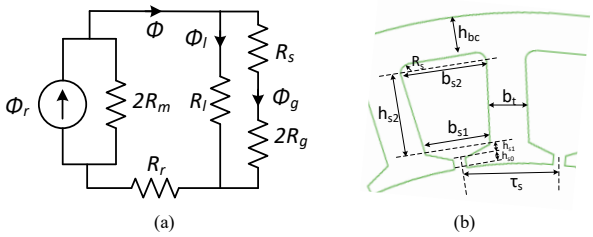

(a) (b)

Figure 6. (a) Electromagnetic lumped parameter magnetic circuit, (b) Slot dimensions

$$B_{gp} = C_\Phi k_l B_r/(1 + K_r \mu_r \, l_g/l_m) \quad (7)$$

$$h_{bc} = \pi e_m D_{is} B_{gp}/(2 \, p \, B_{ys-max}) \quad (8)$$

$$b_t = \pi D_{is} B_{gp} /(Q_s B_{ts-max}) \quad (9)$$

The determination of the number of turns is based on E_{phm} and flux per pole (Φ_{pp}). Φ_{pp} is found using pole area and flux density. Induced voltage on one turn is determined as in (10), where L_a is the axial length and f_r is the mechanical frequency. The number of turns per coil side (N_{cs}) can be found using (11), where l is the number of layers. The phase current of each module is found by assuming that the motor is operated in vector control mode where the induced voltage is always in-phase with the current, as in (12). The electric loading of the machine is verified using the rated phase current as in (13). Once the rated current is established, winding is selected from standard AWG wires with the specified current density limit (J_{rms}). The only remaining parameter on the machine dimensions is the slot height (h_{s2}) as shown in Fig. 6. The limiting factor for h_{s2} is the maximum slot fill factor ($k_{cu\text{-}max}$), as seen in (14). Now, all the dimensions of the machine are set including the stator outer diameter (D_{os}) which is critical for power density.

$$E_{coil} = 4.44 f_r k_w B_{gp} L_a D_{is} \quad (10)$$

$$N_{cs} = 2E_{phm}/(E_{coil} w_s l) \quad (11)$$

$$I_{phm} = P_{out}/(m \, n \, E_{phm}) \quad (12)$$

$$A_{rms} = l\, N_{cs} Q_s I_{phm}/(\pi D_{is}) \quad (13)$$

$$h_{s2} = 2lN_{cs}A_{wdg}/[k_{cu-max}(b_{s1} + b_{s2})] \quad (14)$$

Once all the machine dimensions, winding configuration and turn numbers are set, the machine losses are calculated for the evaluation of the design. Copper loss is directly related to the selected winding cross-section (A_{wdg}) and the mean-length-turn as expressed in (15). The temperature effect is added via the temperature coefficient of copper, where ρ_{cu} is the resistivity of copper for a given temperature. For core loss, the selected lamination (*M250-50A*) is used in several FEA simulations to determine the core loss density with worst case flux density values in several parts of the core. A core loss density of *4 W/kg* is obtained including fundamental and harmonic components and used for core loss calculation.

$$P_{cu} = 2\, m\, n\, {I_{phm}}^2 \rho_{cu}[L_a + \pi^2 D_{is}/(4Q_s) + h_t/2]/A_{wdg} \quad (15)$$

2.3 Thermal sub-model

The thermal model including GaN devices and the lumped parameter thermal circuit used at steady state to determine the maximum heat sink thermal resistance ($R_{th\text{-}sa}$) are shown in Fig. 7. Natural cooling is preferred in the design due to the reliability issues. $R_{th\text{-}sa}$ is calculated as (17) to ensure that the junction temperature of any device do not exceed their maximum values (T_{jmax}). Thermal resistance of PCB and thermal interface material (TIM) are determined using manufacturer's application note [7]. Analytical models are used to determine heat sink dimensions and fin geometry. The fin geometry and physical model of the heat sink is shown in Fig. 8. The thermal resistance of the heat sink is expressed in (18) for natural convection, where A_{base} is the base plate area, A_{fin} is the total fin surface area, η_{fin} is the fin efficiency and N_{fin} is number of fins. The convection coefficient (h) is found using an analytical model derived in [9].

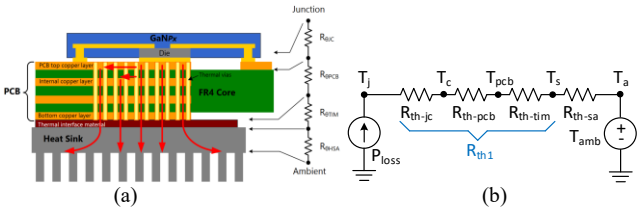

(a) (b)

Figure 7. (a) Thermal model structure [7], (b) Lumped parameter thermal equivalent circuit

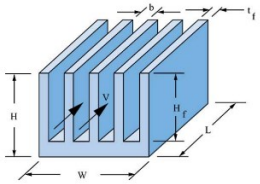

Figure 8. The physical model of the heat sink [9]

$$R_{th-sa-min} = \left(T_{jmax} - T_{amb}\right)/(nP_{loss}) - R_{th1}/n \quad (17)$$

$$R_{th-sa} = \left[h\left(A_{base} + N_{fin}\eta_{fin}A_{fin}\right)\right]^{-1} \quad (18)$$

2.4 Geometrical sub-model

In the geometrical model, main machine dimensions (D_{is}, L_a) are determined using torque per unit volume, A_{rms} and B_{avg}, as expressed in (19). Electric and magnetic loading values are the target parameters specific to natural cooled PMSMs at this power level. The aspect ratio (α=L_a/D_{is}) gives the resultant dimensions. After the capacitors are determined, heat sink and other motor parameters, the objective function, the volumetric power density (PD_v) of the system is calculated using the height of each component and the machine outer diameter as shown in Fig. 2. Moreover, the active material volume and mass for copper, magnet and iron are also calculated.

$$T_m = \pi {D_{is}}^2 L_a A_{rms} B_{avg}/2 \quad (19)$$

3 System evaluation with design parameters

The variables in Table 2 are used to investigate the effect of each design parameter to the system performance indices such as overall system power density, drive and motor efficiency and active material mass.

3.1 The effect of switching frequency

Variation of motor drive efficiency (η_d), total required DC link capacitance (C_{dc}), power density (PDv), and heat sink (V_{hs}), drive (V_{dr}) and total volume (V_{tot}) with switching frequency (f_{sw}) are shown in Fig. 8 for different parallel connected modules (n_p). η_{dr} decreases as f_{sw} increases as expected, however this effect is more severe with low n_p values because switching losses become more dominant than the conduction losses as the GaN current rating increases. Moreover, the relation with number of modules and efficiency is not linear because GaN selection is based on discrete commercial devices which causes underutilization for some cases.

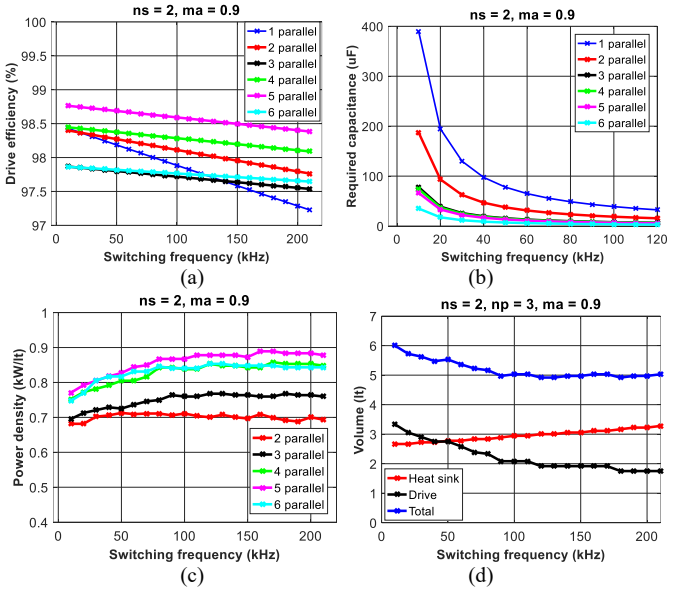

Figure 8. (a) η_d, (b) C_{dc}, (c) V_{hs}, V_{dr} and V_{tot}, (d) PDv variations with f_{sw}

C_{dc} is inversely proportional to f_{sw} as expected. After a certain point, reduction of C_{dc} is not significant, especially for high n_p values. The rms ripple current requirement (I_{crms}) dominates C_{dc} requirement for high f_{sw} in capacitor selection, because f_{sw} has no direct effect on I_{crms}. It is also expected that V_{hs} increases while V_{dr} decreases with increasing f_{sw} values. The effect of f_{sw} to the total volume also saturates after a critical point, which is different for different n_p values. This means that, increasing f_{sw} does not provide further volume reduction above 100 kHz which is also observed in power density variations. Effect of n_p on PDv also saturates after 4 parallel modules as the effect of interleaving also saturates.

3.2 The effect of modulation depth

Variation of η_d, required C_{dc}, I_{crms} and motor efficiency (η_m) with modulation depth (m_a) are shown in Fig. 9 for different n_p values. η_d increases as m_a increases since the same amount of power can be transferred with less current which reduces the conduction losses. However, this effect is not also linear with varying n_p because of the discrete nature of the selected devices. In this analysis, the device selection is based on minimum possible device cost. If this were not considered, very high efficiency values would be obtained, which is not practical. The effect of m_a on C_{dc} is not as severe as frequency, especially for high n_p values. On the other hand, I_{crms} decreases drastically with increasing m_a. Normally, increasing m_a would also yield efficiency reduction due to increasing current, however there is a similar phenomenon in η_m variation with η_d variation, which is caused by the discrete winding selection in the model. η_m does not vary much with varying m_a. Similarly, effect of n_p on η_m is not critical after 2 parallel modules.

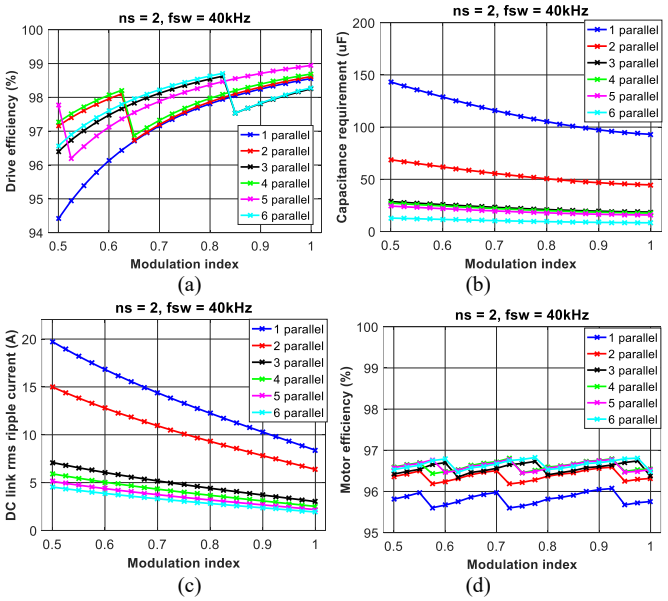

Figure 9. (a) η_d, (b) C_{dc}, (c) I_{crms}, (d) η_m variations with m_a

3.3 The effect of series connection

The variation of C_{dc} and PDv for different number of series (n_s) and parallel (n_p) connected modules are shown in Fig. 10. C_{dc} increases with n_s linearly, which causes volume and cost increase, although n_s has no direct effect on I_{crms}. The volume increase can also be observed on PDv variation. As a result, high number of series connection is not feasible considering also the increased number of devices.

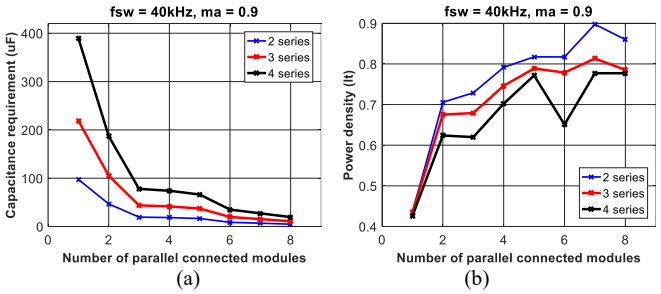

Figure 10. (a) Required C_{dc}, (b) PDv variation with n_s and n_p

3.4 The effect of aspect ratio and number of slots

Variation of η_m, PDv and total motor active material cost (C_m), which includes iron, copper and magnet costs, with aspect ratio (α) are shown in Fig. 11 for different n_p values. Number of slots (Q_s) is directly proportional to n_p as expressed in (k). The first observation from this analysis is that, increasing Q_s after 24 do not have significant effect on any of the performance indices. Moreover, a very high Q_s is not practical as the slot pitch gets very thin. Increasing α has positive effect on the power density, however this effect vanishes after a critical point, which is also different for different n_p values. On the other hand, increasing α decreases η_m and increases C_m almost linearly, which are both disadvantageous. These results suggest that, each n_p has its own optimum α, which is nothing but the aforementioned critical point.

$$Q_s = w\ m\ n_s\ n_p \qquad \text{(k)}$$

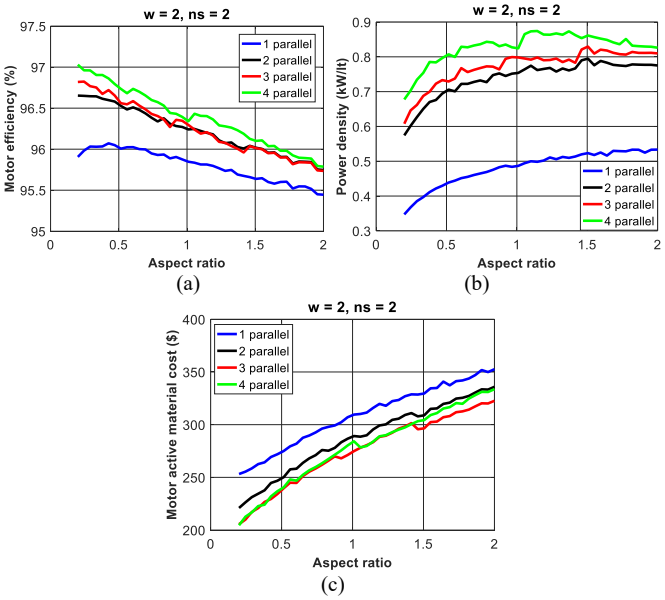

Figure 10. (a) η_m, (b) PDv, (c) C_m variations with α

4 System design and simulation results

Using the results of Sec. 3, an optimum system design is performed for the ratings given in Table 1, and the resulting

system parameters are listed in Table 3. In this section, the design will be evaluated using MATLAB/Simulink for the drive electronics side and ANSYS/Maxwell for the motor side. The proposed analytical model will also be verified using these simulation platforms. The performance of the designed system is shown in Table 4.

n_s is selected as 2, which is the minimum possible value due to the voltage rating of GaNs, since a higher value yields a worse performance in all aspects.

m_a is selected as 0.9 as performance indices are not affected significantly for large m_a values, especially I_{crms} which is highly dependent on m_a. There is a possibility of over-modulation, which may cause loss increase due to injected low order harmonics, in case of voltage sags on the supply, therefore m_a is determined by a margin.

n_p and f_{sw} are considered together since their effects are more inter-dependent. 1 n_p is not feasible for any frequency value in all aspects. The drive efficiency drops below the constraint on drive efficiency for 3 n_p, therefore it is not selected although power density is good. For Icrms, below np<3 is not good, but one should check which parameter is domainant. np = 5 has the best efficiency, however np>= is not feasible for most of the alfa values as the slot pitch gets very thin. np = 4 and 2 has similar efficiency, but np = 4 has very good PDv.

For np = 2, low fsw is feasible such as 50kHz, after that it is not affected much. For np = 4, frequencies up to 100 kHz are feasible.

Designed parameters	**Value**
Number of modules, n	*4*
Number of series modules, n_s	*2*
Switching frequency, f_{sw}	*50 kHz*
Modulation index, m_a	*0.9*
Aspect ratio of the motor, α	*0.5*
Slot/module/phase, w_s	*2*

Table 3. Resulting system parameters

Parameter	**Value**	**Parameter**	**Value**
Drive efficiency, η_{dr}	*Xx %*	Power density, PD_v	*Xy kW/lt*
Motor efficiency, η_m	*Xx %*	Motor cost, C_m	*Xy $*

Table 4. Performance of the designed system

GaN ve cap'ı sözle söyleyelim

Nasıl seçtiğimizi anlatalım (her parametreyi)

Cost'u nasıl dikkate aldık onu belirtelim

Limiting faktörleri anlatalım

5 Conclusions

An 8kW, 540V DC link system is designed using the developed optimization tool.
The resultant system has the performance indices of x kW/lt, x % drive efficiency and y % motor efficiency

İki noktaya vurgu yapalım:
1. Multi-physics
2. Real components

Discrete nature of real components
Çelişkiler
Evrensel ilişkiler
Limitler (fsw şunun üstünde mantıklı değil, max 5 modül feasible gibi)
IMMD'ye özel ilişkiler

Acknowledgements

This work was supported by the Scientific and Technological Research Council of Turkey (TÜBİTAK), Grant No: 117E252 and Middle East Technical University Research Funds, Grant No: BAP-03-01-2017-004.

References

[1] G. Lo Calzo, G. Vakil, B. Mecrow, S. Lambert, T. Cox, C. Gerada, M. Johnson, and R. Abebe, “Integrated motor drives: state of the art and future trends,” *IET Electr. Power Appl.*, vol. 10, no. 8, pp. 757–771, Sep. 2016.
[2] M. D. Hennen, M. Niessen, C. Heyers, H. J. Brauer, and R. W. De Doncker, “Development and control of an integrated and distributed inverter for a fault tolerant five-phase switched reluctance traction drive,” *IEEE Trans. Power Electron.*, vol. 27, no. 2, pp. 547–554, 2012.
[3] J. Wang, Y. Li, and Y. Han, “Integrated Modular Motor Drive Design With GaN Power FETs,” *IEEE Trans. Ind. Appl.*, vol. 51, no. c, pp. 3198–3207, 2015.
[4] M. Ugur and O. Keysan, “DC link capacitor optimization for integrated modular motor drives,” *2017 IEEE 26th Int. Symp. Ind. Electron.*, vol. i, pp. 263–270, 2017.
[5] A. Shea and T. M. Jahns, “Hardware integration for an integrated modular motor drive including distributed control,” in *2014 IEEE Energy Conversion Congress and Exposition (ECCE)*, 2014, pp. 4881–4887.
[6] N. Bekka, M. E. H. Zaim, N. Bernard, and D. Trichet, “A Novel Methodology for Optimal Design of Fractional Slot with Concentrated Windings,” *IEEE Trans. Energy Convers.*, vol. 31, no. 3, pp. 1153–1160, 2016.
[7] GaN Systems, “GaN Systems.” [Online]. Available: http://www.gansystems.com/. [Accessed: 15-Jan-2018].
[8] TDK, “Film Capacitors, Metallized Polypropylene Film Capacitors (MKP) - B32674...B32674 Datasheet,” no. May. 2015.
[9] R. E. Simons, “Estimating Parallel Plate-Fin Heat Sink Thermal Resistance.” [Online]. Available: https://www.electronics-cooling.com/2003/02/estimating-parallel-plate-fin-heat-sink-thermal-resistance/.